April, 1981

Interaction of a compressional impulse with a slot normal to the surface of an elastic half space — II

A. Ilan
Leonard J. Bond

Geophys. J. R. astr. Soc. (1981) **65**, 75–90

Interaction of a compressional impulse with a slot normal to the surface of an elastic half space – II

A. Ilan* and L. J. Bond† *Department of Physics, The City University, London*

Received 1980 May 9; in original form 1979 October 23

Summary. An improved finite difference scheme has been used to simulate the propagation of a plane *P*-impulse in an elastic half space with a slot normal to its surface. Various angles of incidence and dimensions of slot are considered. The numerical results are presented in several visualizations; each emphasized a different type of wave and all representations help in understanding the scattered and diffracted wave pattern. Experiments were carried out using 0.5–6 MHz ultrasonic pulses on a duralumin semidisc with a surface-breaking slot and the results are compared with those given by the numerical models.

The scattered wavefield includes compressional and Rayleigh pulses whose amplitude increases at the front of the slot and decreases behind it, as the angle of incidence is reduced. A diffracted compressional pulse is generated with a semicircular wavefront centred at the mid-point of the bottom of the slot. Also, two elliptical eddies are excited at the lower corners. These ellipses propagate into the medium and eventually spread out to form arc-shaped shear pulses.

In the shadow zone, behind the slot, the two components of displacement show independent behaviour. The horizontal component decreases either with decreasing angle of incidence or as the slot is made deeper. For acute angles, a reduction of displacement amplitude of about 50 per cent is obtained when the depth of the slot is made a half pulse width. On the other hand there is no diminution of the vertical displacement behind the slot, and, near the upper right corner, it is even amplified.

Introduction

Several research projects have investigated the ground motion in the neighbourhood of prominent irregularities, due to incident *SH*-waves. However, the more complicated problem

* Formerly with the Department of Geophysics and Planetary Sciences, Tel-Aviv University, and now returned to Israel.

† Now in the Department of Electronic and Electrical Engineering, University College London, London WC1.

of *P–SV*-wave propagation, in similar models has far fewer solutions. Gangi (1967) and Gangi & Wesson (1978) experimentally determined the *P*-wave to Raleigh-wave conversion coefficients at stress-free wedges. A numerical solution by Bouchon (1973) studied the effect of depressions and ridges on surface motion. The interaction of elastic waves with surface waves has also been investigated experimentally in electronics, by a number of workers including Humphryes & Ash (1969) and, more recently, Parekh & Tuan (1977).

Ilan, Bond & Spivack (1979) (henceforth paper 1) studied the surface motion and the scattered and diffracted wave pattern due to a plane *P*-pulse, propagating, in a half space with a slot normal to its surface. This paper presents an extension of that work: while Paper 1 concentrates on a normally incident *P*-pulse, the present paper considers various angles of incidence e, and studies the effect of e, on the various phases of the scattered and diffracted waves (Fig. 1). Various slot dimensions are considered and the shielding effect of the slot is evaluated.

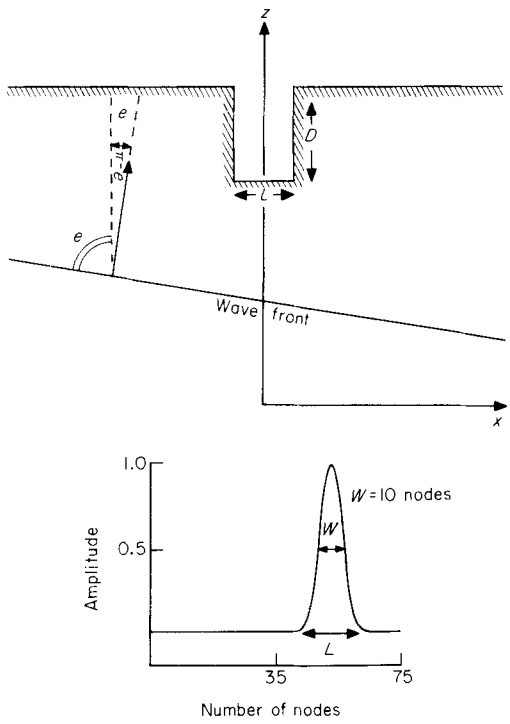

Figure 1. Cross-section of the model.

The medium is assumed to be perfectly elastic, isotropic and homogeneous. A square grid of order 70×70 and spatial grid increment K has been imposed around the slot. The displacements of the inner (body) points are calculated by the use of a scheme used by Alterman & Loewenthal (1970), where the derivatives are replaced by central finite differences. The displacements at the corners are calculated using the formulae of Alterman & Loewenthal (1970) and Ilan, Ungar & Alterman (1975). The free surface boundary conditions are approximated by the new composed scheme by Ilan & Loewenthal (1976).

These approximations are all of second-order accuracy and the formulation produced is an explicit three-level finite difference scheme.

Excitation

The excitation on the half space is assumed to be a plane P–SV-pulse. The shape of the pulse is the δ function $\langle\delta(\xi)\rangle$ (Fig. 1), smoothed as described in Paper 1:

$$\langle\delta(\xi)\rangle = [G_5(\xi+5\Delta) - 5G_5(\xi+3\Delta) + 10G_5(\xi+\Delta) - 10G_5(\xi-\Delta) + 5G_5(\xi-3\Delta) - G_5(\xi-5\Delta)]/(230\Delta^4) \quad (1)$$

where

$$G_5 = \xi^4/4!\, H(\xi). \quad (2)$$

H is the Heaviside step function and Δ is an arbitrary parameter which determines the pulse width. In the calculations the pulse was spread over 18 grid points. Let α, β be the compressional and the shear wave velocity respectively and $\beta/\alpha = 0.575$. Let e, f be the angles of the reflected compressional and shear waves respectively. The displacements (U^i, W^i) are those which would occur if the surface were flat as given by Ewing, Jardetsky & Press (1957).

$$U^i = \frac{\cos e}{\alpha}\,[\delta\langle t-(x\cos e + z\sin e)/\alpha\rangle + A\,\delta\langle t-(x\cos e - z\sin e)/\alpha\rangle] + \frac{\sin f}{\beta}\,B\,\delta\langle t-(x\cos f - z\sin f)/\beta\rangle \quad (3)$$

$$W^i = \frac{\sin e}{\alpha}\,[\delta\langle t-(x\cos e + z\sin e)/\alpha\rangle - A\,\delta\langle t-(x\cos e - z\sin e)/\alpha\rangle] + \frac{\cos f}{\beta}\,\beta\delta\langle t-(x\cos f - z\sin f)/\beta\rangle, \quad (4)$$

where A, B are the reflection coefficients,

$$A = \frac{4\tan e\tan f - (1+3\tan^2 e)^2}{4\tan e\tan f + (1+3\tan^2 e)^2} \qquad B = \frac{-4\tan e\,(1+3\tan^2 e)}{4\tan e\tan f + (1+3\tan^2 e)^2}.$$

The model is a half space with a normal slot (Fig. 1). A grid of the order 70×70 was imposed on the model around the slot. The displacements at the first two time steps for all grid points were determined by equations (3) and (4). (For the subsequent time steps the displacements at the inner points of the grid and the stress-free surface were calculated by the finite difference scheme described in Paper 1.) On the three artificial boundaries of the grid (U^i, W^i) given by equations (3) and (4) were imposed at every time step. The use of the analytical solution at the edges of the grids provides the exact solution of the problem up to the time when the first scattered wave arrives at the artificial boundaries. Stopping the calculation at this time step, and by using a sufficiently large grid, guarantees that the artificial reflections resulting from the use of a finite grid do not contaminate the results.

The surface displacements

The surface motion in the vicinity of the slot due to P-pulses of various angles of incidence was studied. The maximum amplitudes of the two components of displacements at 20 observation points were divided by the respective amplitudes at the plane free surface. The

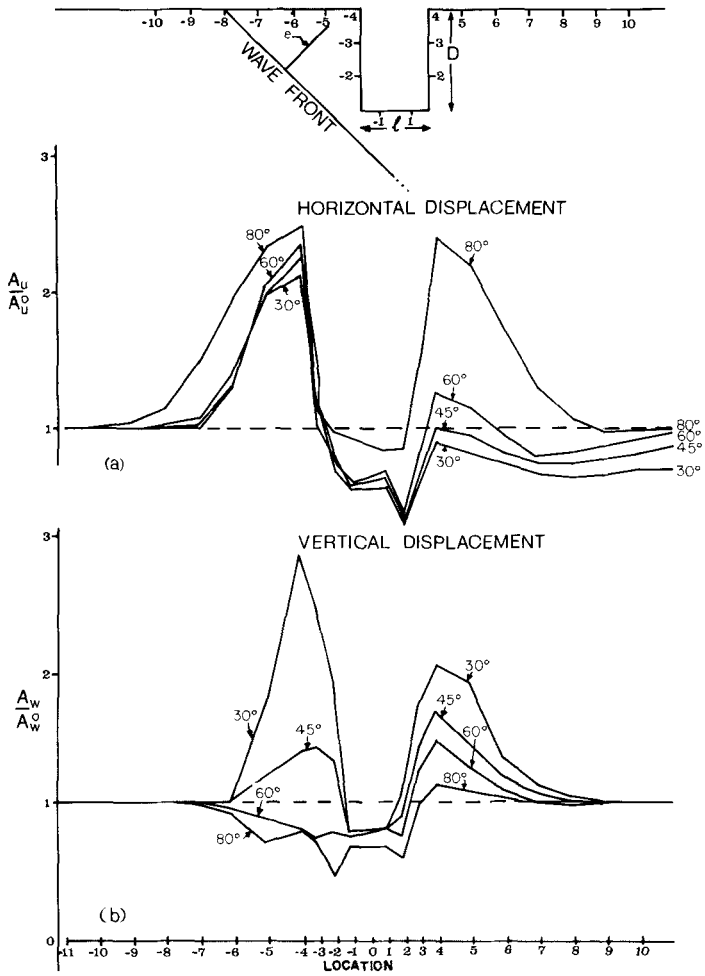

Figure 2. A_u/A_u^0 and A_w/A_w^0 at 20 observation points on the surface around a slot, as indicated above. Here A_u, A_w are the horizontal and vertical displacement amplitudes due to *P*-pulses at various angles of incidence A_u^0, A_w^0 are the respective amplitudes of a *P*-pulse at a flat surface. Here $l = L/3$, $D = L/4$ where L is the width of the pulse.

relative amplitudes are depicted in Figs 2 and 3. In Fig. 2 the depth (D) and the width (l) of the slot are $L/3$ and $L/4$ respectively. The angle of incidence was varied over the values $e = 30°, 45°, 60°$ and $80°$, measured as positive in the counter-clockwise direction from the x-axis. Thus, $e = 0$ corresponds to a grazing wave approaching from the left side and $e = 90°$ is a normal incidence. In Fig. 3 the angle of incidence and the width of the slot are constants, $e = 45°$ and $L/4$ respectively, while the depth of the slot varied, $D = L/3$, $L/2$, $3L/4$. These figures show that the effect of the discontinuity on the surface motion due to a *P*-pulse differs in some aspects from the effect of discontinuity on *SH*-waves, investigated by Trifunac (1973) and Wong & Trifunac (1974) and others. The horizontal component of displacement is amplified by approximately a factor of 2 at the upper left corner of the slot, and decreases rapidly along the left flank and along the bottom of the slot. The horizontal displacement becomes a minimum at the lower part of the right flank. A shadow zone exists

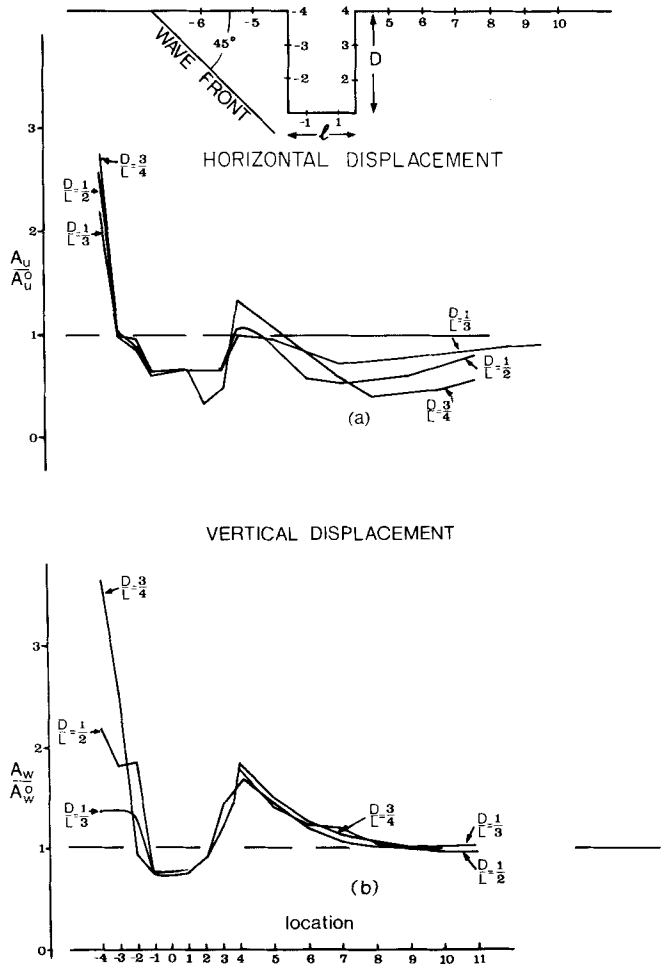

Figure 3. Relative amplitudes at 16 observation points, as defined in Fig. 2. Here the angle of incidence is 45° and the depth of slot varied, $D = L/3$, $L/2$ and $3L/4$.

behind the slot, which becomes wider and deeper as the slot itself is made deeper or the angle of incidence sharper. For the cases of $e = 45°$, when the slot width l is $2L/9$ and the slots depth D varied, $D = L/3$, $L/2$, $3/4L$, the minimum relative horizontal displacement has been found to be 0.74, 0.52 and 0.40 respectively. For the case where $D = L/3$, $l = 2L/9$ and $e = 80°$, 60°, 45° and 30°, the minimum horizontal amplitude is found to be 0.99, 0.81, 0.74 and 0.65 respectively. Generally, the behaviour of the horizontal component on the irregularity is similar to that of an *SH*-pulse. On the other hand, no diminution of the vertical component behind the slot was found. Near the upper right corner it was even amplified, and the amount of amplification increased as the angle of incidence was made smaller. When the slot was made deeper (from $L/3$ to $3L/4$) the amount of amplification decreased by only 16 per cent. The last result is of some practical interest as the slot may be a model of a trench. It appears that a trench may reduce the horizontal but not the vertical ground motion.

Fig. 4 shows a cross-section of a half space where a *P*-pulse strikes the surface at 30°, which is the critical angle of incidence at which the total energy is converted to a reflected

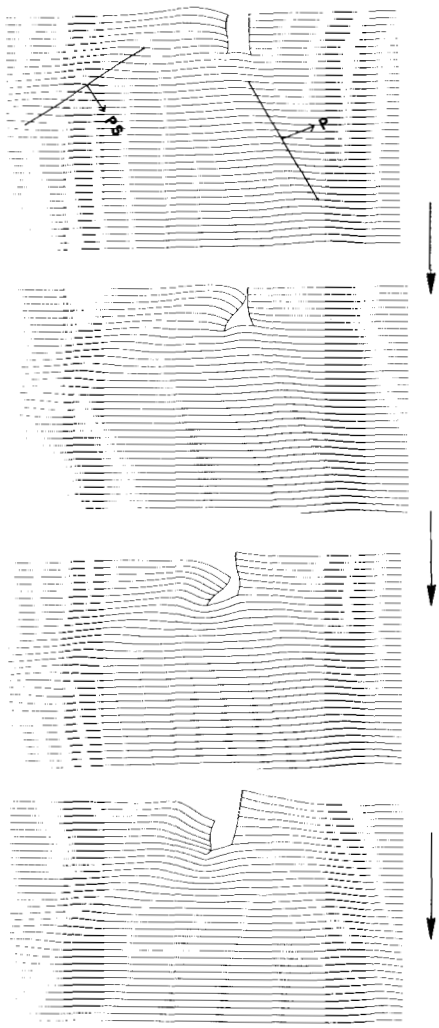

Figure 4. Cross-section of the model at four consecutive times, $t\alpha/h = 16$, 20, 24 and 28. The angle of incidence is 30° and the slot dimensions are: $D = L/3$, $l = 2L/4$.

shear pulse. The amplitudes of the displacements were amplified in the visualization for emphasis and the position of particles at all grid points were connected by horizontal lines. The figure shows the main lines of distortion of the slot surface, that of the right flank being mainly a vertical stretching while the left one shows considerable bowing downwards and to the right. While being pulled back by the elastic forces the left flank excites a high amplitude pulse propagating to the left, like a bow releasing an arrow. (The dynamic behaviour of the slot is vividly shown when the model results are used to generate 16 mm film (Ilan 1978).)

The scattered and diffracted waves

In Fig. 5 the wavefront is at 35° to the slot and displacements have been amplified further to reveal even small distortions. Two pulses with 180° phase delay between them are shown

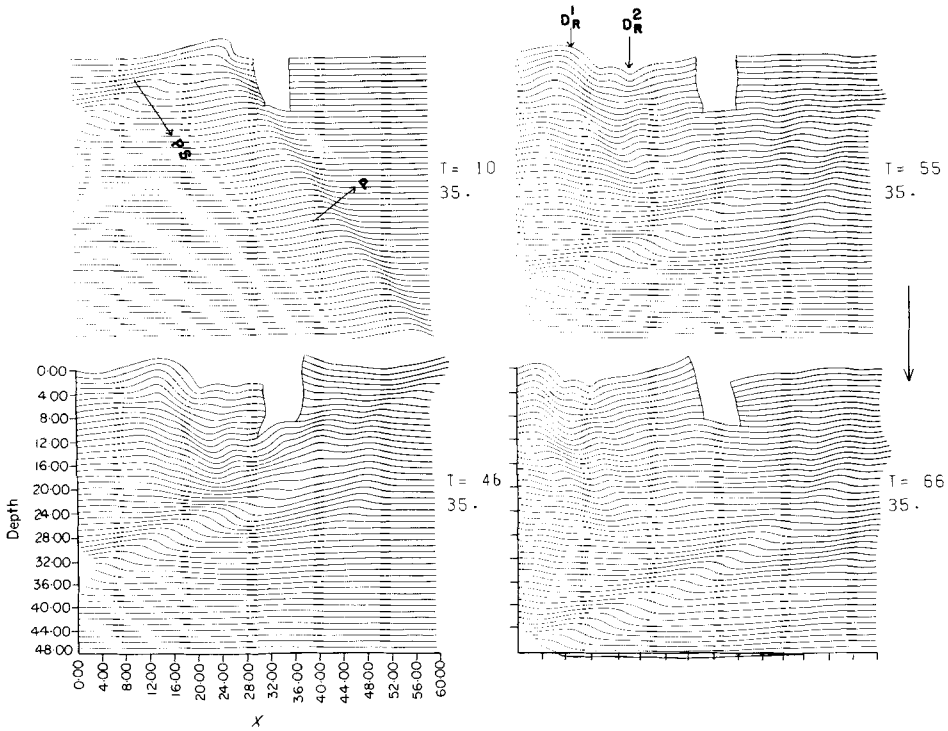

Figure 5. Cross-section of the model at four time levels due to a *P*-pulse incident at 35°. The times are given by the first number in each figure. The dimensions of the slot are, $D = L/2$, $l = L/3$. D_R^1 and D_R^2 on the Rayleigh waves referred to in the text.

which propagate with Rayleigh-wave velocity from the slot towards the left side. Two arc-shaped wavefronts are also observed around the lower corners. While running the program whose solutions are depicted in Fig. 5, displacements at 16 grid points along the surface were stored. The components of these displacements were later plotted as functions of time, as shown in Fig. 6. This representation enables us to observe the arrival times of a certain type of wave at a series of recording points and so to determine its wave velocity. For this case, after the arrival of the initial pulse the region behind the slot is relatively quiet while on the left side, in front of the slot, several disturbances can be seen. The horizontal components in Fig. 6 show a compressional pulse scattered to the left with a wavefront parallel to the vertical flanks. The vertical components show the two Rayleigh pulses with an 80° phase delay. These have already been detected in the cross-section depicted in Fig. 5. Similar calculations were made for various angles of incidence. It was found that with decreasing angle of incidence the amplitude of the scattered Rayleigh wave increased linearly in front of the slot and decreased behind it. Fig. 7 shows the components of displacements as functions of time. Here the observation points were chosen at a depth L (equal to the pulse length) below the surface. This figure shows, beside the original *P–SV*-waves, a shear pulse which has been diffracted from the lower right corner of the slot. In Figs 8, 9 and 10 the results of consecutive time steps are represented in a manner adapted from Harumi, Saito & Fujimori (1978). The displacements, the sizes of which have been doubled in the figure for emphasis, are represented by a vector at every grid point, showing the direction of displacements relative to the direction of propagation, and the shapes of the wavefronts of the different modes. The representation adapted from Harumi *et*

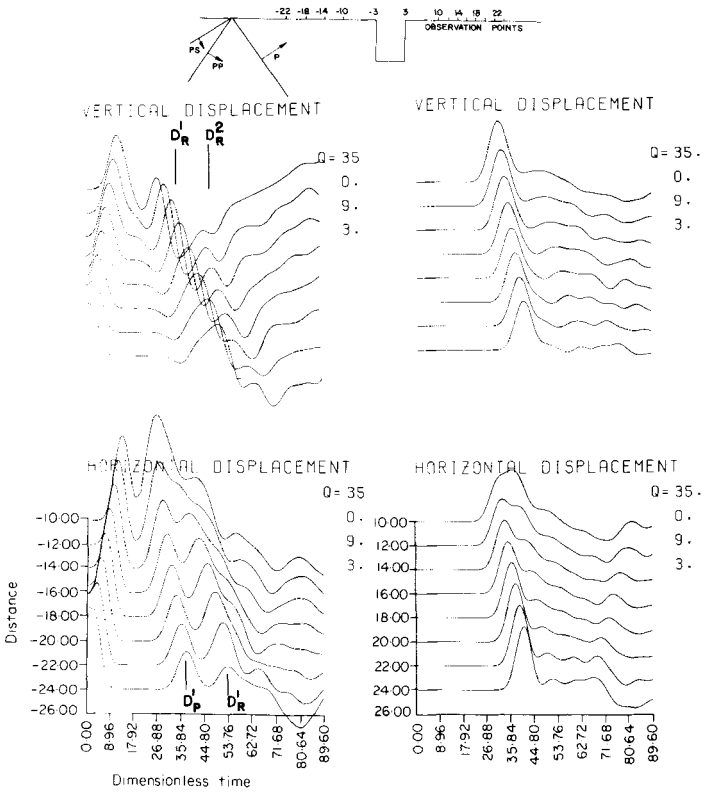

Figure 6. Displacements due to a plane *P*-pulse at 35° incidence as functions of $t\alpha/h$. The observation points are on the surface of both sides of the slot as indicated above. The dimensions of the slot are $D = L/2$, $l = L/3$; D_P^i, D_S^i, D_R^i, $i = 1, 2$ are the scattered compressional, shear and Rayleigh waves respectively.

al. (1978) appears to be the best means for identifying the different wavefronts of the scattered waves. In Fig. 8 the incident initial pulse is normal to the surface $e = 90°$, and therefore the scattered wave pattern is symmetrical. This figure includes cross-sections at six different time steps. In the first cross-section (Fig. 8a) the compressional pulse has already arrived and has been normally reflected. In addition, a compressional diffracted pulse can be seen propagating in a semicircular wavefront centred at the mid-point of the bottom of the slot. Later two arc-shaped shear pulses are diffracted from the lower corners. Also Rayleigh pulses are seen to propagate from the upper corners, along the horizontal and vertical surfaces, the characteristics of these waves being clearly shown (e.g. the retrograde elliptical motion of the particles, the vanishing of the horizontal component at a depth of about 0.19 wavelengths and the change of its direction of motion at greater depths). In the next view (Fig. 8b) the reflected pulse has already been diffracted around the lower corners. In the shadow zone, the amplitude of this diffracted pulse is reduced and its phase delayed relative to the reflected *P*-pulse. Elliptical eddies have also been excited at the lower corners, where the directions of displacements are counter-clockwise in the left ellipse and clockwise in the right. Both ellipses have advanced in the direction of 45° and 135°. These ellipses become spread out later and form arc-shaped wavefronts. Harumi *et al.* (1978), in their simulation of elastic waves from a transducer, also noticed elliptical motion and accounted for it by an

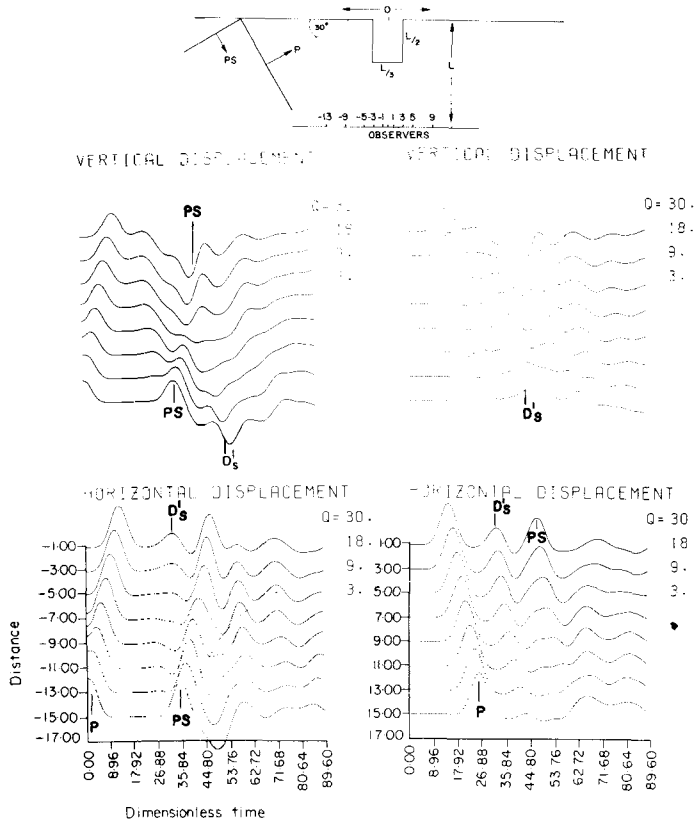

Figure 7. Displacements due to a plane *P*-pulse at 30° incidence as functions of $t\alpha/h$. The observation points are at a depth L below the surface, as indicated. The other details are as in Fig. 6.

interaction of compressional and shear waves. In Figs 9 and 10 the angles of incidence are 70° and 45° respectively and the wave patterns are obviously non-symmetric. The amplitudes of Rayleigh pulses increase on the left side of the slot and decrease on the right when the angle of incidence is sharpened. When the initial pulse is diffracted around the right corner, the direction of displacements is changed and becomes nearer to the vertical flank. The ellipses are excited at different times, and both rotate counter-clockwise. The first is generated at the lower right corner, after it has been hit by the incident pulse. The second ellipse is excited at the left corner after having been hit by the reflected compressional pulse.

Description of experiment

To test the results given by the numerical models a series of laboratory experiments were performed to observe the scattered waves generated when ultrasonic pulses (0.5–6 MHz) are incident on slots cut into duralumin blocks.

The use of ultrasonic waves in models to investigate propagation in seismological systems has been reported by several workers and an extensive treatment of the basic principals involved is given by O'Brien & Symes (1971).

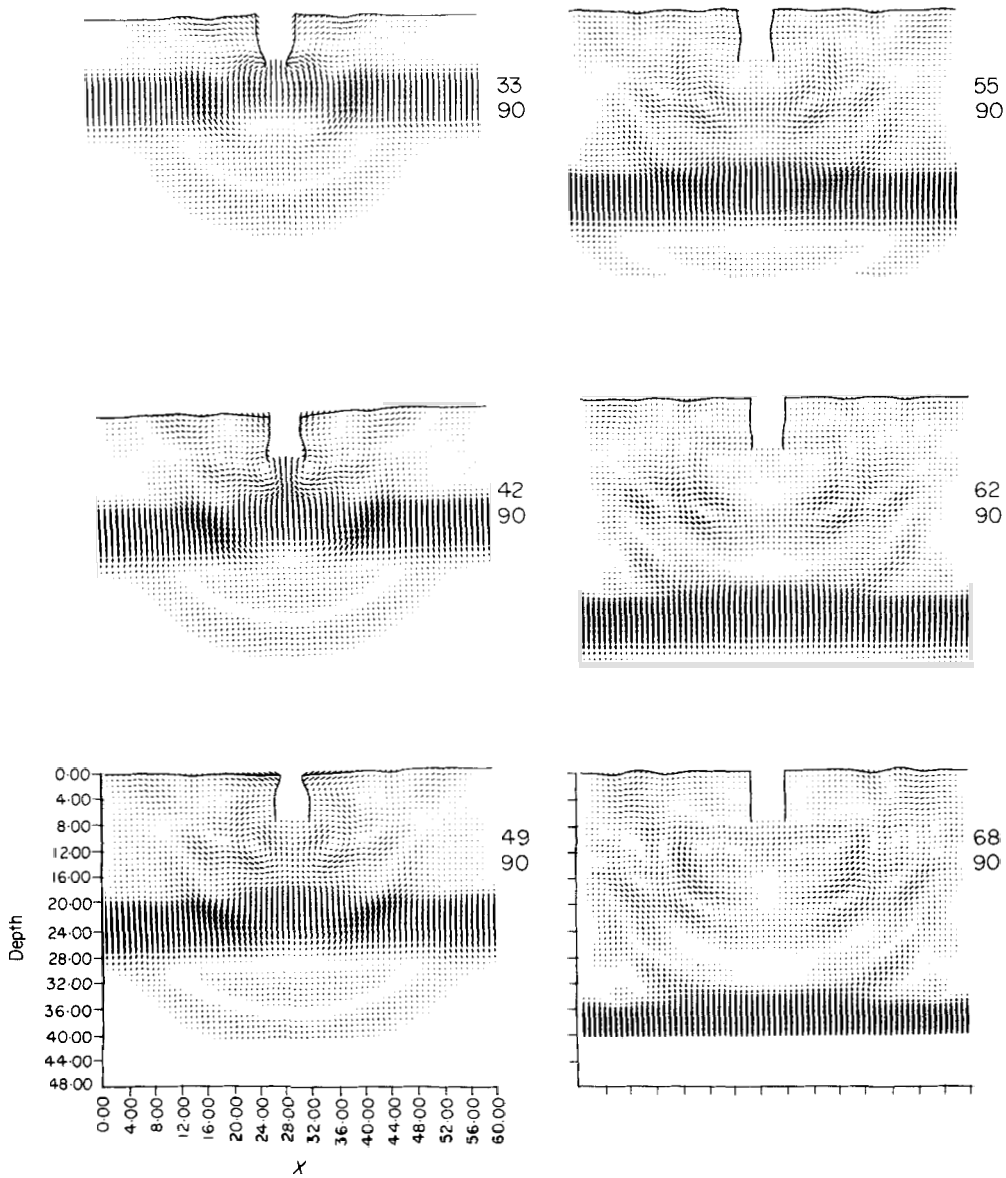

Figure 8. Cross-sections of the model at six consecutive time steps. The times in units of h/α are indicated by the upper number in each subfigure and the lower number is the angle of incidence. The dimensions of the slot are $D = L/2$, $l = L/3$, and the size of displacements was doubled in the graph.

The experimental system used in this study was based on ultrasonic equipment which is used for non-destructive testing (Brown & Weight 1974; Bond 1978).

The ultrasonic waves used were generated by conventional piezoelectric transducers, driven by a pulse generator. The receiving system consisted of an ultrasonic surface wave transducer connected to a wide-band amplifier which was in turn connected to a display system to give either the time domain signal ('seismogram') or spectrum of the received pulse, and x–y plotter.

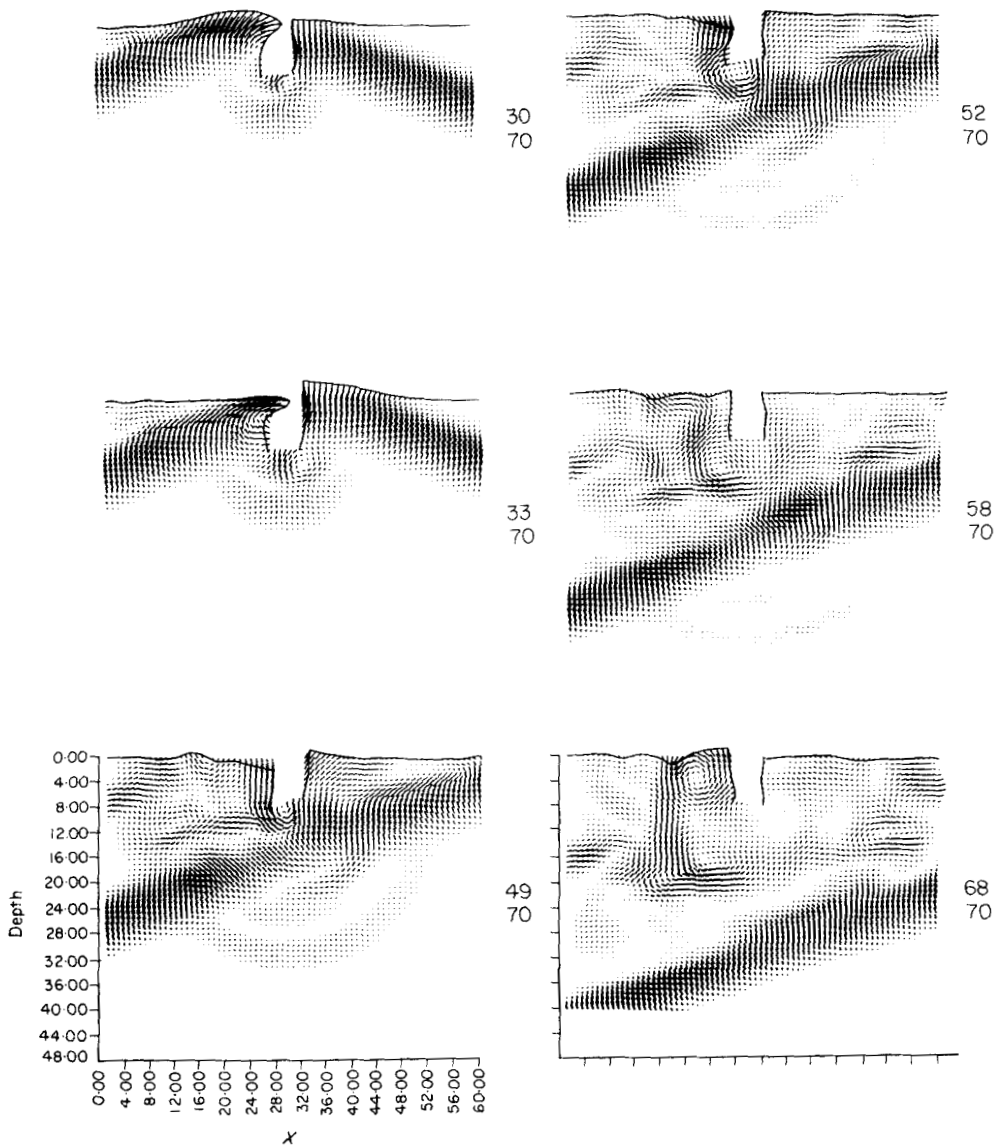

Figure 9. Cross-sections of the model due to a plane *P*-pulse at 70° incidence. The other details are as in Fig. 8.

The experimental arrangement giving the basic transducer positions on the test block is shown as Fig. 11.

A slot (1 mm wide and 2 mm deep) was cut normal to the flat surface, and along the axis of a semidisc. The circular surface of the semidisc at the angles 30°, 45°, 60° and 90° was flattened to make small planes perpendicular to the radius. The block was placed in a water bath to the depth shown in Fig. 11. The water both acts as the coupling medium and increases the pulse path length which simplifies analysis.

The pulses generated by a 3 cm diameter compression wave transducer were first investigated using a semidisc without a slot, and a second compressional transducer placed on the

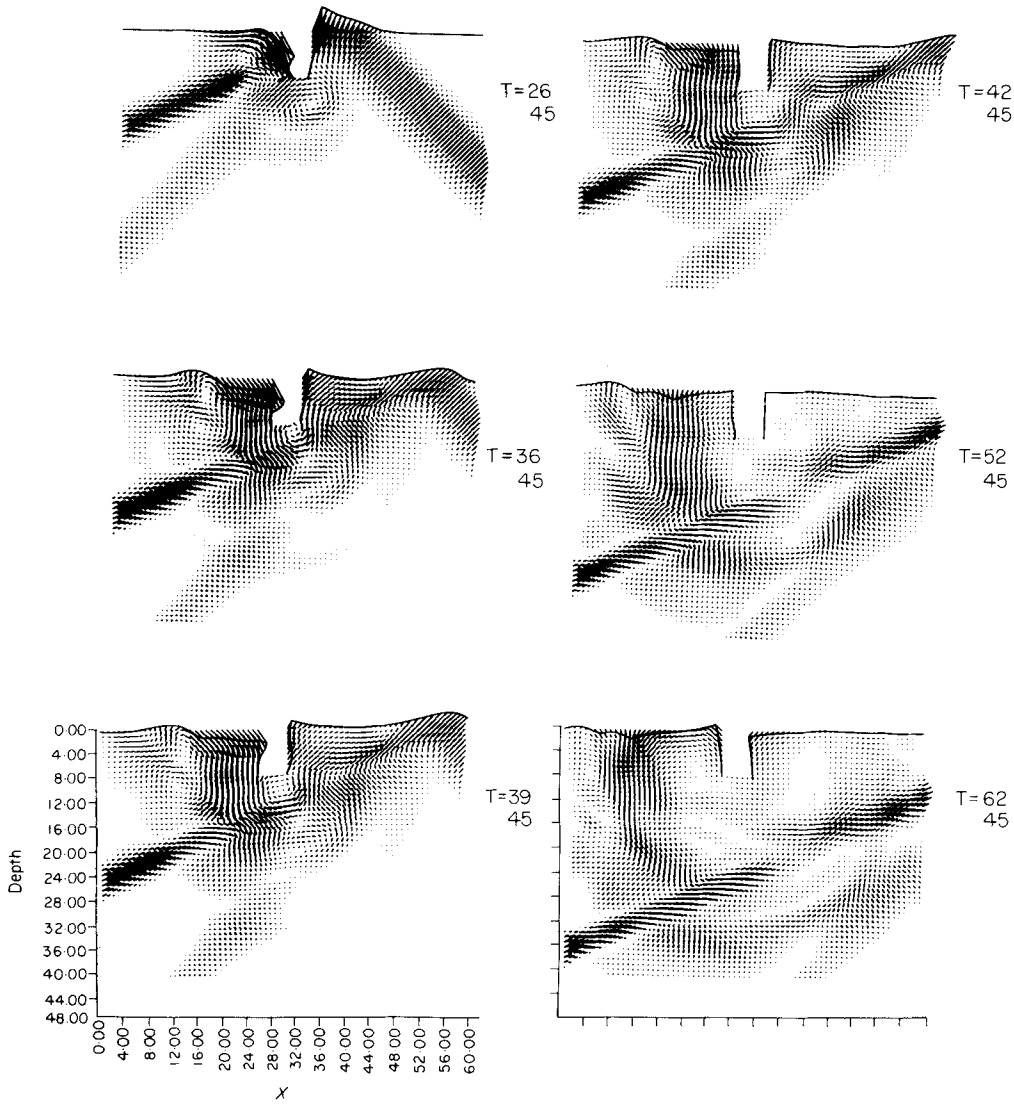

Figure 10. Cross-sections of the model due to a plane *P*-pulse at 45° incidence. The other details are as in Fig. 8.

flat surface of the block. The incident pulse was measured using the second transducer and the pulse frequency content was found to be centred around 2.5 MHz. As the compressional wave velocity of the duralumin was 6230 m s^{-1} the pulse wavelength was about 2.5 mm. The compressional pulse, as measured using the second compressional transducer, is shown in both time and frequency domains as Fig. 12(a).

The waves in the semidisc containing the slot were then investigated. The cylindrical transducer of 3 cm diameter was carefully aligned opposite the small planes on the semidisc and used to generate compressional waves in the block, the transducer being set in turn in the positions A to E shown in Fig. 11.

A wedge transducer sensitive to Rayleigh waves was carefully bonded to the flat surface of the block, once on the left and once on the right side of the slot, for each transmitter position, and the scattered and mode-converted pulses were investigated.

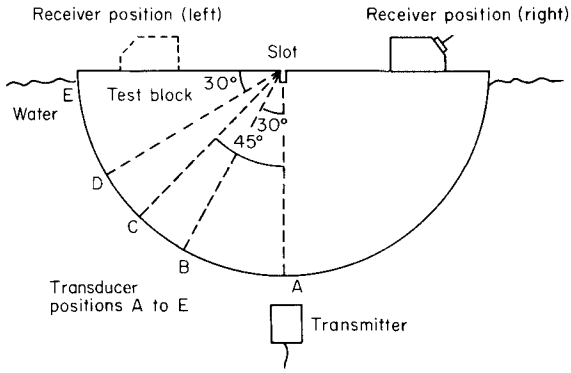

Figure 11. Diagrammatic picture of the experiment.

For each position of the transmitter the compressional pulse was partly transmitted into the block and this energy hit the slot at the chosen angle. The scattered pulses of Rayleigh waves were detected by the wedge transducers and for each angle of incidence the time domain signals were recorded. The time domain signals and spectra for the case of 45° angle of incidence, on both sides of the slot, are shown as Fig. 12(b, c). The spectra of the scattered Rayleigh waves were found to contain lower frequencies than those of the initial pulse, the spectra being centred around 1.25 MHz.

The results of the experiment were plotted and, for each angle of incidence, the amplitudes of the scattered Rayleigh pulses were normalized to that for $e=90°$. The

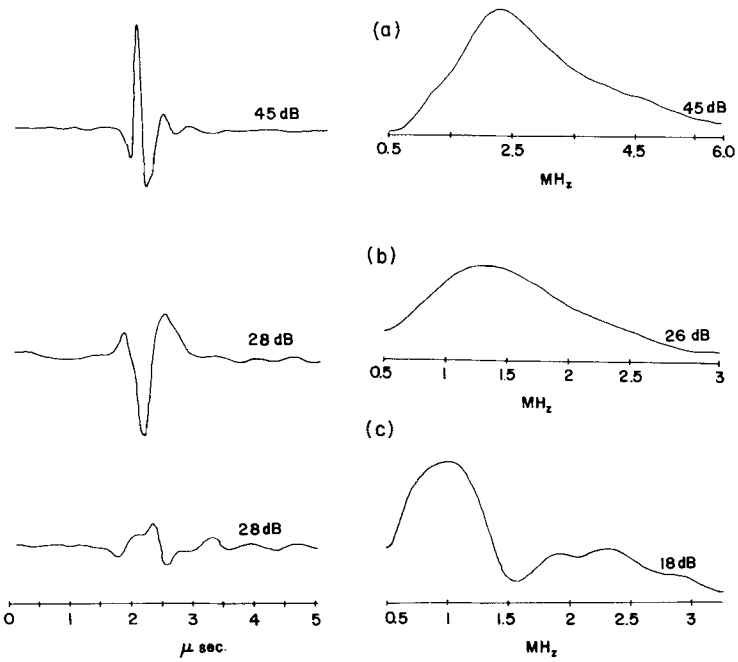

Figure 12. Representative results of the experiment described in Fig. 11. The vertical displacements as functions of time on the left side and the amplitude spectrum on the right. (a) The normally *P*-pulse reflected from a flat surface. (b), (c) The scattered Rayleigh pulses due to a *P*-pulse incidence at 45°, (b) at the front of the slot, (c) behind the slot. The depth and width of the slot are 2 and 1 mm respectively.

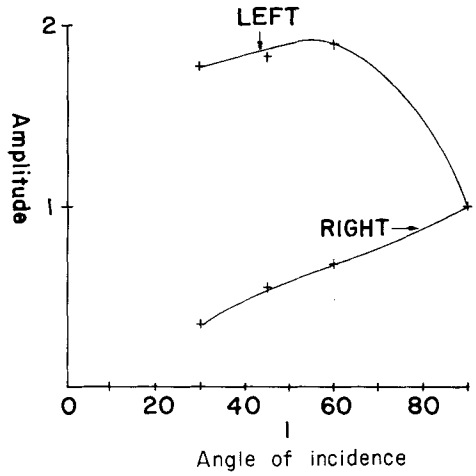

Figure 13. Experimental values of the normalized amplitude of the scattered Rayleigh pulse due to a compressional pulse of various angles of incidence at both sides of the slot.

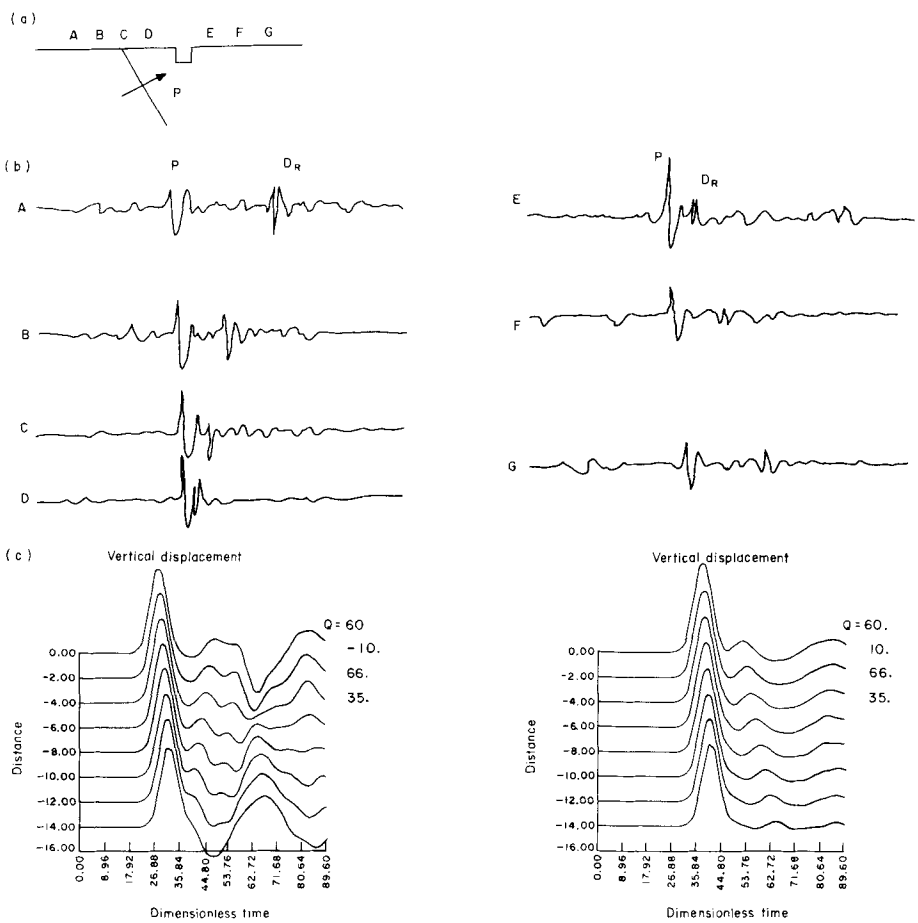

Figure 14. Experimental and numerical surface displacements for *P*-pulse at 60° and with observation points on both sides of the slot.

normalized amplitudes, as a function of angle of incidence, are shown in Fig. 13. On the left side of the slot the amplitude is almost doubled when $e = 60^\circ$ and decreases slightly for $e = 45^\circ$ and 30°. On the right side, behind the slot the amplitude of the Rayleigh waves decreases linearly with e. A maximum in the amplitude of the scattered Rayleigh waves was observed at $e = 60^\circ$ and for this case a series of further experiments were performed. The basic transducer configuration was the same as for the earlier measurements, being that shown in Fig. 11, with the transmitter in position C. In addition, the wedge transducer was replaced with a special transducer used to detect the vertical component of displacement, which is a modified form of the design given by Harnik (1977), due to Bond (1978). The receiving transducer was placed in a series of positions moving across the flat surface of the block (Fig. 14a) and at each position the time domain signal was recorded. The resulting traces are shown in Fig. 14(b) together with the results of the numerical model for the same angle of incidence (Fig. 14c). For the cases of receiver positions A to D the incident *P*-wave is seen to move from left to right along the trace (later arrival time) and agrees well with the numerical model results. A mode-converted pulse (D_R) is seen to move in the opposite direction to the *P*-wave across these traces. When the velocities of this pulse in both the experimental and numerical results are measured, they are found to be the Rayleigh-wave velocity. There is good agreement between the two results both for the velocities and the pulse energy content relative to the incident pulse.

For the traces E to G, in Fig. 14, the incident *P*-wave pulse is again seen to move from left to right, as shown in the numerical model. In both sets of results, a mode-converted pulse is observed to follow the *P*-wave pulse but at a much slower velocity. For both the numerical model and the experiments the velocity of this pulse was determined and found to be in good agreement with the Rayleigh-wave velocity. In addition, the energy content of the scattered pulses, relative to the incident pulse, were again in good agreement.

There are also several low-energy pulses to be found in both the numerical model and experimental results.

Conclusions

The experimental results are generally in good agreement with the numerical ones, and this work has provided further understanding in the complex problem of the scattering of elastic waves by slots.

Two differences between numeral results and experiments have been found, both of which can be explained. These are, first, that the amplitude pattern of Rayleigh waves on the left of the slot, according to the numerical results, has the amplitude increase linearly with decreasing angle of incidence. In the laboratory, the amplitude increases considerably when e decreases from 90° to 60° – but it decreases slightly when e is made even smaller. This effect is believed to be due to the difference between the numerical and experimental initial pulses, which have infinite and finite widths respectively. This assumption is to be tested by further computations, assuming plane pulses with finite dimensions, and by further experiments. The second difference is that two consecutively scattered Rayleigh pulses can clearly be distinguished in the numerical results, but only one pulse appears in the experimental results, and this is believed to be due to a combination of background noise and attenuation which occur in the experiments.

Acknowledgments

This work forms part of a programme of research which seeks to provide an adequate theory for the understanding of elastic wave scattering problems. The authors were supported by

the Natural Environment Research Council and Procurement Executive, Ministry of Defence (UK) respectively, and thank the two organizations for their respective Research Fellowships. Thanks are due to all the members of the group at the City University who have helped in this work, especially Mr J. P. Weight, Senior Experimental Officer, for his help in carrying out the experiments, and Professor A. F. Brown (TCU) and Mr A. L. Downie (University College London) for their help in the preparation of this paper, and also to Mrs S. Adler, Department of Geophysics, Tel-Aviv University, for editing the original manuscript of this paper.

References

Alterman, Z. S. & Loewenthal, D., 1970. Seismic waves in a quarter and three-quarter plane, *Geophys. J. R. astr. Soc.*, **20**, 101–126.

Bond, L. J., 1978. Surface cracks in metals and their characterisation using Rayleigh waves, *PhD thesis*, The City University, London.

Bouchon, M., 1973. Effect on topography on surface motion, *Bull. seism. Soc. Am.*, **63**, 615–632.

Brown, A. F. & Weight, J. P., 1974. Generation and reception of wideband ultrasound, *Ultrasonics*, **12**, 161–167.

Ewing, W. M., Jardetsky, W., Press, F., 1957. *Elastic Waves in Layered Media*, McGraw-Hill, New York.

Gangi, A. F., 1967. *J. geophys. Res.*, **72**, 5685–5692.

Gangi, A. F. & Wesson, R. L., 1978. *P*-wave to Rayleigh-wave conversion coefficients for wedge corners; model experiments, *J. comp. Phys.*, **29**, 370–388.

Harnik, E., 1977. A broadband probe for studies of acoustic surface waves, *J. Phys.*, **10E**, 1217–1218.

Harumi, K., Saito, T. & Fujimori, T., 1978. Motion picture of the computer simulation of elastic waves from transducer, *FASE-78 Proc. Vol II*, pp. 51–60, Warszawa Polish Academy of Sciences.

Humphryes & Ash, 1969. Acoustic bulk-surface wave transducers, *Electronics Lett.*, **5**, 175–176.

Ilan, A., 1978. Compressional plane impulse at a half-space, *film* produced by the City University, Department of Physics.

Ilan, A., Bond. L. J. & Spivack, M., 1979. Interaction of a compressional impulse with a slot normal to the surface of an elastic half-space, *Geophys. J. R. astr. Soc.*, **57**, 463–477.

Ilan, A. & Loewenthal, D., 1976. Instability of finite difference schemes due to boundary conditions in elastic media, *Geophys. Prosp.*, **24**, 431–453.

Ilan, A., Unger, A. & Alterman, Z. S., 1975. An improved representation of boundary conditions in finite difference schemes for seismological problems, *Geophys. J. R. astr. Soc.*, **43**, 727–742.

O'Brien, P. N. S. & Symes, M. P., 1971. Model seismology, *Rep. Prog. Phys.*, **34**, 697–764.

Parekh, J. P. & Tuar, H. S., 1977. Reflection and bulk – wave conversion of Rayleigh wave at a single shallow groove, *J. Appl. Phys.*, **48E**, 994–1003.

Trifunac, M. D., 1973. Scattering of plane SH waves by a semi-cylindrical canyon, *Int. J. Earthqu. Eng. Struct. Dym.*, **1**, 267–281.

Wong, H. L. & Trifunac, M. D., 1974. Scattering of plane SH waves by semi-elliptical canyon, *Int. J. Earthqu. Eng. Struct. Dym.*, **3**, 157–169.